Physics of the Solid State, 2022, Vol. 64, No. 11

03,10

Quantum-chemical study of structure and vibrational spectra of Si/SiO_2 superlattices

© M.B. Smirnov[1], D.V. Pankin[1], E.M. Roginskii[2], A.V. Savin[2]

[1] St. Petersburg State University,
St. Petersburg, Russia
[2] Ioffe Institute,
St. Petersburg, Russia
E-mail: m.smirnov@spbu.ru

Received July 9, 2022
Revised July 9, 2022
Accepted July 11, 2022

Structure, phonon states and vibrational spectra of binary Si/SiO_2 superlattices (SL) formed by junction of crystalline silicon and β-cristobalite are investigated with the use of ab-initio quantum-mechanical computational methods. Several stable SL structures with ultra-narrow interfaces consisted of only one monolayer of Si^{2+} atoms are found. For these SLs, we have simulated the infrared and Raman spectra in which some characteristic spectral features are detected.

Keywords: oxide-semiconductor heterostructures, superlattices, computer simulation, density functional method, vibrational spectra.

DOI: 10.21883/PSS.2022.11.54190.430

1. Introduction

The key element of MOS transistors, which is the most commonly used in modern electronics, is the oxide-semiconductor interface. The silicon-based electronics mainly uses SiO_2 as an oxide. The requirement of miniaturization sets out technologists to produce ultrathin oxide layers, which actualizes the problem of understanding the laws that control the formation of interfaces at the level of atoms. Understanding of the structure-properties relation is impossible without theoretical research based on high-precision calculations of the electron structure. Today the most reliable methods to simulate the electron structure of condensed media are based on the calculations with the scope of density functional theory. The use of these calculations for studying the structure and properties of heterostructures with Si/SiO_2 interfaces has a long history (see [1] and references therein). In most of these studies, the flat interface of Si/SiO_2 was simulated using superlattices (SL), i.e., periodic layered heterostructures. This technique allowed for the use of methods developed for 3D periodic structures to simulate 2D interfaces. While initially SLs used as convenient simulation systems to simulate flat Si/SiO_2 heterojunctions, later, when these systems were synthesized and their experimental studying was started, it was found that they possess unique electronic, dielectric, and optic properties that determine their promising potential for the creation of new optoelectronic devices [2]. Since then a lot of papers were published based on results of experimental and theoretical studies of Si/SiO_2 SL properties (see [3–5] and references therein).

It is worth noting, that previous theoretical studies were devoted to the spatial and electron structure of Si/SiO_2 SL. The issue of the nature of vibration states of these systems was out of the scope of theoreticians. However, the experimental data gained by now as related to vibration spectra (Raman spectra first of all) of these systems is indicative of the existence of a fundamental correlations between structural, vibrational, and electron characteristics of these objects. Raman spectroscopy has proved its efficiency as a very informative and sensitive method of the non-destructive analysis of structures of semiconductor nitride superlattices. It was shown in a number of studies, that the analysis of the Raman spectra makes it possible to estimate to a high precision the thickness of layers, quality of interfaces, and tensions in layer materials. In application to SL of Si/SiO_2, the use of the Raman spectroscopy [6–11] made it possible to obtain valuable information on the structure of layers and on the temperature impact on crystallization processes, to estimate crystallite sizes, and to get information on the presence and value of stresses. The most precision study [12] with the use of information of frequency positions of spectral lines corresponding to spatially limited acoustic phonons has managed to estimate the thicknesses of layers in the grown SLs. However, so far nobody had conducted a detailed theoretical analysis of the obtained spectra on the basis of strict quantum-mechanical calculations. This paper presents the results of a theoretical study of vibration spectra of one of the possible types of Si/SiO_2 SL, which can be considered as the first step towards comprehensive study of the structure-spectrum relation for these heterostructures, which are important from the practical point of view.

Structure and properties of the Si/SiO_2 interface were targets of many theoretic studies based on computer simulation using the method of density functional [13–31]. The key problem of this kind of research activities was the choice of a suitable structural model of the interface layer. As a rule, in real samples the oxide layer is in an amorphous state. Since there are certain difficulties in simulating the amorphous state for theoretical analysis, the calculations used different polymorphic modifications of crystalline silica, such as christobalite [13–14,16–19,24,26–28], quartz [17,19,21,25,30], or tridymite [15,17,19,20]. Taking into account that most of the studies used christobalite, we decided to start with a model based on this structure.

2. Calculation procedure

In the calculations of the electron structure, we used a variant of the density functional theory — the generalized gradient approximation (GGA) with PBEsol functional [32] implemented in the ABINIT software package [33–35]. Main electron states of atoms were described using a norm-conserving pseudopotential [36]. In this case $3s3p$ states of Si atoms and $2s2p$ states of O atoms were considered as valence states. The plane wave basis was build up with a cut-off energy of $E_c = 45$ Ha. A set of k-points in the Brillouin zone was defined by the Monkhorst–Pack scheme [37] with a density of $6 \times 6 \times 2$. Self-consistency criterion in the solution to the electron problem was defined as 10^{-8} Ha. Parameters of the lattice were optimized to residual stresses of 0.01 GPa, while atom sites were optimized to residual forces of 10^{-5} Ha/Bohr. Frequencies and shapes of center-zone vibrations, as well as IR and Raman scattering (RS) intensities were calculated using the perturbation theory [38,39].

3. Results and discussion

When choosing a spatial model for the Si/SiO_2 SL, the most frequently used are the interfaces formed by (001) surfaces of silicon crystals and β-christobalite (see Fig. 1, a and b). This approach is attributable to the fact that these two crystalline structures have identical symmetry, and Si atoms in them occupy identical sites. The only difference between them is that in the oxide there is an O atom between two neighboring atoms of Si. If orientations of two lattices are the same, then the interface area is extremely thin being composed of only one layer of Si atoms forming two Si−Si bonds in the silicon layer and two Si−O bonds in the oxide layer. However, there were serious doubts related to the stability of this interface because cell sizes of two structures are significantly different: the cell of β-christobalite is by 35% greater than the silicon cell. Therefore, in [13] it was suggested to align the surfaces of two lattices by rotating one of them by 45° when building up the interface. With this orientation linear dimensions of two lattices become close to each other, but a half of interface atoms of Si appear to have two of four bonds being cut off. Different relaxation mechanisms for this structural defect were discussed in a number of works [13,14,16,24,26]. The general conclusion comes down to the understanding that with this method of structures juncture the interface becomes blurred, i.e., includes several layers of silicon atoms with different degrees of oxidation.

It is worth reminding, that the main objective of the simulation is to search for a structure with interface blurred to the minimum possible extent. Therefore we decided to return back to the initial model and start the search for a stable heterostructure on the basis of the SL with sharp interface, that is the structure arising from the juncture of silicon lattice with christobalite lattice without rotation by 45°. Taking into account that without structural rebuilding such a structure is indubitably unstable, we decided to study all possible variants of its structural relaxation. Due to labor intensity of the calculation process, we decided to start with a relatively short-period SL with layers containing crystal cells of Si and β-christobalite doubled in the direction of heterostructure growth. This structure, being composed of 4 monolayers of Si interleaved with 4 monolayers of SiO_2, can be designated as $Si_4/(SiO_2)_4$. It has a symmetry corresponding to point group D_{2d} and space group $P\bar{4}m2$ (#115). We determined the initial size of a heterostructure cell in the plane of interface $a = 4.547$ Å as an average value between cell sizes of Si (3.84 Å) and β-christobalite (5.25 Å). We assumed the cell size and atom sites in the normal direction (that is layer thicknesses and distances between monolayers) equal to their values in unstressed bulk crystals. Summarized cell constant was $c = 12.86$ Å. By optimizing the geometry with the saved symmetry, we obtained a structure with the cell stretched in the interface plane ($a = 4.908$ Å) and compressed along the SL axis ($c = 12.021$ Å) (see Fig. 1, a).

The calculation of phonon spectrum of the structure #115 has shown the presence of four modes with imaginary frequencies: two nondegenerated modes of symmetry A_2 and B_1 with frequencies of $172i$ cm^{-1} and $86i$ cm^{-1} and two modes of symmetry E with frequencies of $147i$ cm^{-1} and $122i$ cm^{-1}. The analysis of eigenvectors of these modes has shown that they all are localized in the oxide layer and composed mainly of rotations of SiO_4 tetrahedrons. In the lattice dynamics such modes are known as the Rigid Unit Modes (RUM). There are many different RUMs in the structure of bulk β-christobalite. They all are unstable. Detailed analysis of different structures arising from β-christobalite at relaxation over different RUMs is presented in [40].

Searching for a stable configuration, we distorted structure #115 by the eigenvector of each unstable mode and optimized the geometry. Having optimized the structure distorted by mode A_2, we obtained a new structure with a symmetry corresponding to space group $P\bar{4}$ (#81), which appeared to be stable. Having optimized the structure distorted by modes of type E, we obtained a new structure with space group Pm, and optimization of the structure

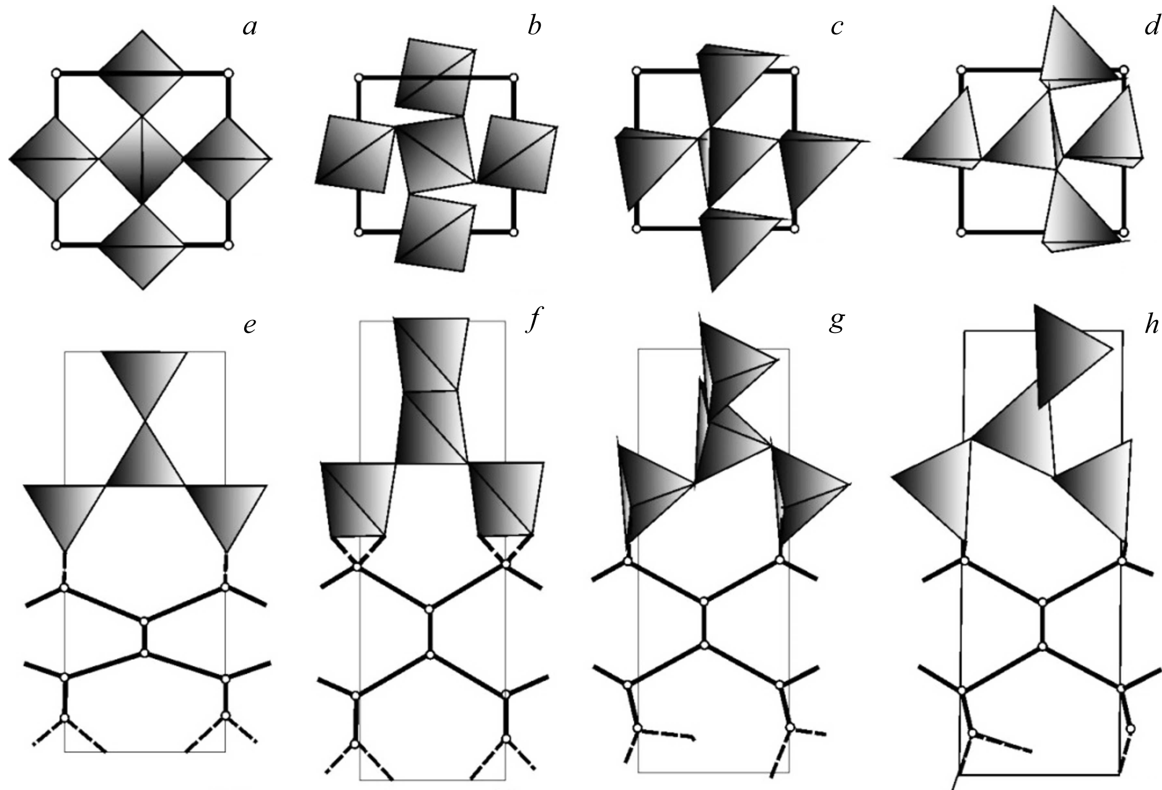

Figure 1. SL structures with a symmetry of #115 (*a, e*), #81 (*b,f*), #5 (*c, g*), and #1 (*d, h*) space groups in xy (*a–d*) and xz (*e–f*) projections.

distorted by the mode of type B_1 gave us a new structure with space group $C222$. However, both these structures appeared to be unstable. We were forced to repeat the relaxation procedure: distorted them by eigenvectors of unstable modes and optimized the geometry with a setting of a lower symmetry. At the second stage we have succeeded to find two new low-symmetry structures $C2$ (#5) and $P1$ (#1) without modes with imaginary frequencies in their phonon spectra. All found stable structures are shown in Fig. 1.

Mode A_2 with a frequency of $172i\,\text{cm}^{-1}$ is composed of rotations of SiO_4 tetrahedrons about axes parallel to the axis c. Similar distortion in the crystal of β-christobalite transfers it into a modification known as $\tilde{\beta}$-christobalite [41] with space group of symmetry $I\bar{4}2d$ (#122). Therefore we can consider the $P\bar{4}$ (#81) SL as a sandwich, where silicon layers have a structure of crystalline silicon oriented with axis (001) in the direction of SL growth, and oxide layers have a structure of $\tilde{\beta}$-christobalite with its main axis in the direction of SL growth (see Fig. 1, *b*).

Other unstable modes are composed of rotations of SiO_4 tetrahedron about axes normal to the axis c. The character of these rotations can be seen most explicitly in figures of the top row in Fig. 1. It can be seen that in SL #5 (see Fig. 1, *c*) in the oxide layer structure the tetrahedrons are rotated in the same manner as in SL #81, but the axis of rotation corresponds to the direction of $(\bar{1}10)$. Exploring the properties of oxide with this structure, we have to appeal to $\tilde{\beta}$-christobalite again.

In SL #1 (see Fig. 1, *d*), a part of tetrahedrons in the structure of oxide layer are rotated about axes directed along $(\bar{1}10)$, while another part are rotated about normal axes (110). Similar RUM-distortion of β-christobalite results in structure $P2_1nb$ (#33) [40]. Nobody has observed such modification of christobalite in bulk samples.

The lowering of energy obtained in three possible scenarios of relaxation is different insignificantly: it is -2.179, -2.344, and -2.247 eV/cell for structures #2, #1, and #81. The lowest energy corresponds to the most low-symmetry structure $P1$. Perhaps, it is this type of SL, that is the most suitable for the simulation of heterostructures with an amorphous oxide layer. Energy of SL #81, which is the most symmetric among stable structures, is just by ~ 6 meV/atom higher, which is comparable with the thermal energy at a room temperature. Taking into account the insignificant difference of energies, we decided to start the study from a detailed analysis of the most symmetric structure among the found structures. It is the SL #81 that is considered in the rest of this paper.

In the SL under consideration, the silicon layer contains 4 monolayers of Si atoms, while the oxide layer contains 4 layers of Si atoms interleaved with four layers of O atoms. The silicon layer is a cell of Si crystal, which is doubled in direction (001). Oxide layer is a cell of $\tilde{\beta}$-christobalite

Table 1. Structural parameters of SL $Si_4/(SiO_2)_4$ (#81)

Parameters of SL	a(4.2024 Å)	b(4.2024 Å)	c(13.2936 Å)
Coordinates of atoms	x	y	z
Si1	0.	0.	0.6920
Si2	0.	0.5	0.8504
Si3	0.5	0.5	0.
Si6	0.	0.5	0.4047
Si7	0.5	0.5	0.5
O1	0.1643	0.7479	0.7731
O3	0.2505	0.3249	0.9251

doubled in direction (001) as well. Parameters of optimized structure SL #81 are listed in Table 1.

The obtained values of cell parameters allows estimating the deformations in SL materials arising when the cell is formed. For this purpose it is necessary to know sizes of cells in unstressed crystals. Our calculations for a unit cell parameter of Si crystal yielded an estimate of $a(\text{Si}) = 5.43$ Å, that matches the experimental data [41]. After optimization of $\tilde{\beta}$-christobalite structure, we obtained the following cell parameters: $a(\text{SiO}_2) = 4.928$ Å and $c(\text{SiO}_2) = 7.269$ Å, that match well the results of previous calculations (5.031 and 7.247 Å [43]) and the experimental data (5.042 and 7.131 Å [44])

According to Table 1, SL cell size in the interface plane is $a(\text{SL}) = 4.2024$ Å. In a bulk unstressed crystal of Si this value corresponds to 3.84 Å. Thus, we come to the conclusion that in the SL under consideration Si layers in the interface plane are stretched by 9.4%. The position of interfaces along the axis c is determined by the planes that pass through atoms of Si1, which relative z-coordinates are equal to 0.308 and 0.692. Hence, the thickness of the silicon layer is $c(\text{Si}) = (0.692 - 0.308) \times 13.2936 = 5.1047$ Å. Comparing this value with the cell constant of a silicon crystal, we come to the conclusion that in the SL under consideration Si layers are compressed by 6% in the direction of heterostructure growth.

By comparing values of a parameter in SL and in unstressed $\tilde{\beta}$-christobalite, we come to the conclusion that the oxide layer is compressed by 17% in the interface plane. The thickness of the oxide layer in SL is $c(\text{SiO}_2) = c(\text{SL}) - c(\text{Si}) = 8.1889$ Å. By comparing this value with the c parameter of unstressed $\tilde{\beta}$-christobalite, we come to the conclusion that in the optimized SL geometry the oxide layers are stretched by 13% in the direction of heterostructure growth. Generally the volume of material in oxide layers is reduced by 22%. It is worth noting, that such strong compression of the oxide structure in the interface plane is reflected in considerably reduced (as compared with unstressed material) angles Si$-$O1$-$Si $= 126^\circ$ and Si$-$O2$-$Si $= 130^\circ$ as compared with 145° in an unstressed crystal of $\tilde{\beta}$-christobalite.

Proceeding with numerical simulation of SL vibration spectra, first of all we calculated phonon states in the crystals that form the layers of heterostructure, i.e., in silicon crystals and in $\tilde{\beta}$-christobalite. For this study of $Si_4/(SiO_2)_4$ superlattices having each layer containing two cells of each crystal, phonon state are of special interest in both the center and the and the boundary of the Brillouin zone in the direction of SL growth: for silicon it is the direction of $\Gamma - X$, while for $\tilde{\beta}$-christobalite it is the direction of $\Gamma - M$. These results are given in Table 2. Calculated distributions of phonon state density are shown in Fig. 2.

Comparison of our results with results of previous studies and experimental data makes it possible to estimate the adequacy of the calculation scheme used. Values of phonon frequencies calculated by us for the silicon crystal match well with results of previous calculations [45] and experiment [46]: our calculated frequencies in average are just 4% lower than the experimental values. There is no experimental data for phonon frequencies of $\tilde{\beta}$-christobalite, but there is a calculation [40]. By comparing our results with this calculation, we have found that our estimates of valence vibration frequencies are higher by $50-80\,\text{cm}^{-1}$. Quality of two calculations can be compared by frequencies in the B_1-E triplet arising from the RS-active T_g-mode of cubic β-christobalite at tetragonal distortion. According to the data of the Raman experiment [46], frequency of this mode is $777\,\text{cm}^{-1}$. In our calculation, frequencies in the B_1-E triplet are equal to $778-792\,\text{cm}^{-1}$, while in [40] these frequencies are $737-748\,\text{cm}^{-1}$. This suggests that our results match the experiment better. It can be assumed that underestimates for phonon frequencies in the calculation of [40] are a consequence of overestimate of lattice parameters.

We have calculated the spectrum of center-zone phonons in the $Si_4/(SiO_2)_4$ SL. The calculated frequencies are shown in Table 2 in comparison with frequencies of component materials.

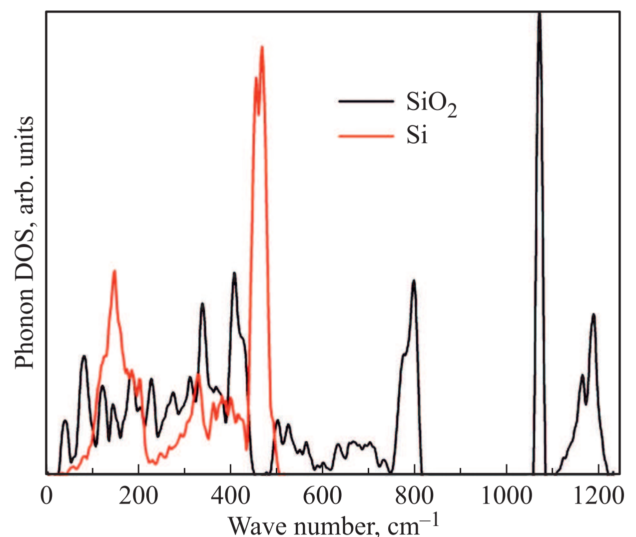

Figure 2. Phonon state density in crystals of silicon and $\tilde{\beta}$-SiO_2

Table 2. Calculated frequencies (in cm^{-1}) of phonon modes in the Si$_4$/(SiO$_2$)$_4$ SL as compared with phonons of component crystals

Group	Attribution	Si$_4$/(SiO$_2$)$_4$			SiO$_2$		Si	
		A	B	E	Γ	M	Γ	X
1	ν_{as}(Si–O)	1157 1028	1114 1029	999 957	1147 A_2 1126 E 1116 B_2	1177 M_5 1071 M_{34}		
2	ν_s(Si–O)	696	791 608	811 720	792 E 778 B_1	798 M_{12} 595 M_s		
3	$\delta(\text{SiO}_2) + \nu(\text{Si–Si})$	547 464 423 393	458 449 427 417	453 398 387	440 E 417 B_2 409 B_1 352 A_2	376 M_s	502 T_{1g}	444 X_4 396 X_1
4	Modes of the lattice	349 180	318 202	323 256 193 123 96 58	316 A_1 89 E	335 M_{34} 317 M_{12} 279 M_5 28 M_{34}		141 X_3

Proceeding with the analysis of phonon states in the SL, first of all we consider the possibility of vibrations localized in individual layers. The main condition of vibrations mixing is proximity of their frequencies. It can be seen from the data presented in Table 2 and in Fig. 2, that phonons in the silicon oxide are distributed over three frequency intervals: frequencies of valence ν(Si–O) vibrations are in the interval of 1060–1200 cm^{-1}, frequencies of deformation vibrations of $\delta(\text{SiO}_4)$ are in the interval of 400–800 cm^{-1}, so called lattice modes fall into the interval below 400 cm^{-1}. It can be seen in Fig. 2, that phonon frequencies in the Si crystal are approximately equally distributed in the interval of 0–520 cm^{-1}. Based on these facts, the following two conclusions can be made:

1. Modes over 600 cm^{-1} should be localized in layers of SiO$_2$. With these frequencies atoms of the silicon layer are practically motionless.

2. Intensive mixing of vibrations is possible at frequencies below 520 cm^{-1}. At frequencies higher than 400 cm^{-1}, the mixed modes can be participated by phonons of the optical zone of silicon crystal, while at lower frequencies the existence of delocalized acoustic phonons is possible.

In accordance with frequencies, we have split the phonon modes of SL into 4 groups. The group of high-frequency modes (950–1200 cm^{-1}) is formed by the modes that include oscillations of O atoms along Si–O–Si bridges. The second group (550–800 cm^{-1}) is formed by the modes that include oscillations of O atoms transversally to Si–O–Si bridges. The third group (350–500 cm^{-1}) is formed by both valence vibrations of atoms in the Si lattice and deformation vibrations (changes of O–Si–O angles) in the oxide material. The low-frequency group (below 350 cm^{-1}) is formed by the modes that are combinations of vibrations of acoustic branches of both materials, so called lattice modes. Only the first and the second groups are clearly separated from others. The boundary between the third and the fourth groups is arbitrary.

When comparing phonon frequencies in SLs and in bulk unstressed crystals, account must be taken of the impact of stresses arising in materials of layers during heterostructure growth. The above analysis of deformations has shown that the material in silicon layers is compressed in the direction of the SL axis and stretched in the interface plane. The impact of anisotropic deformations on phonon frequencies is described using empirical relationships. These relationships for silicon were investigated in a number of studies [48,49]. It was found that the relation between the tension-compression deformation ε_{xx} and frequency offset caused by this deformation $\Delta\omega$ meets the linear law $\Delta\omega = X\varepsilon_{xx}$ in a wide range. Coefficients of this relation were estimated for the Raman-active mode in the Si crystal: $C = -733\,\text{cm}^{-1}$ for biaxial stretching deformation in the interface plane and $C = -337\,\text{cm}^{-1}$ for uniaxial stretching deformation in a direction normal to the interface [48]. In the SL in question the layers of Si are stretched in the interface plane by 9.4% and compressed by 6% in the direction of the SL axis. Using the above values of empirical parameters, we can estimate the frequency offset of phonons localized in Si layers as follows

$$\Delta\omega = -0.094 \cdot 733 + 0.06 \cdot 337 = -49\,\text{cm}^{-1}. \quad (1)$$

The reduction of atom vibration frequency of silicon layer atoms matches the fact that the material of the silicon layer is stretched in the SL. Consequently, taking into account the fact that the material of oxide layer in the SL is compressed, it can be assumed that vibration frequencies of atoms in this layer should increase. However, results of the calculation presented in Table 2 do not confirm this assumption. It

can be seen that frequency intervals of phonons of the first and the second groups in the SL and in the $\tilde{\beta}$-christobalite are nearly coincident. And as for the phonons of the third and the fourth groups with mixed character, it is difficult to separate the effect of stresses from the effect of delocalization. Complex, nonmonotonic behavior of the phonon frequencies dependence on stresses in the christobalite is a consequence of structural lability related to the presence of a large number of RUMs [50]. In particular, as can be seen from the comparison in Fig. 1, a and b, the compression of oxide material in the SL is accompanied by an increase in the sizes of SiO_4 tetrahedrons.

Correlations of phonon states in the SL and component crystals were analyzed using the theory of symmetry groups. The expansion in irreducible representations (IRR) of phonons in Γ- and X-points of a cubic crystal of silicon (point group O_h) is as follows

$$6\Gamma = T_{2g} + T_{1u}(x, y, z) \quad 6X = X_1 + X_3 + X_4. \tag{2}$$

Similar expansion of phonons in Γ- and M-points of the $\tilde{\beta}$-christobalite crystal (point group D_{2d}) is as follows

$$18\Gamma = A1_{+}2A_2 + 2B_1 + 3B_2(z) + 5E(x, y)$$

$$18M = 2M_{12} + 3M_{34} + 4M_5. \tag{3}$$

Phonons in the Γ-point of $Si_4/(SiO_2)_4$ SL (point group S_4) are distributed over three IRRs:

$$48\Gamma = 9A + 11B(z) + 14E(x, y). \tag{4}$$

It is worth reminding, that in equations (2–4) IRRs of types E, X_i and M_i are doubly-degenerated, and IRRs of type T are triply-degenerated. The symmetry group of SL is a subgroup of symmetry groups of component crystals of silicon and $\tilde{\beta}$-christobalite. Theoretical-group analysis in combination with the analysis of vibration waveforms resulted in a correlation of irreducible representations of phonons in the Γ-point of SL and phonons from various points of the Brillouin zone of component crystals. The result is shown in Table 3.

It follows from the obtained scheme, that center-zone phonons A_1 and A_2 of the oxide fall into one A representation of the SL, and center-zone phonons B_1 and B_2 fall into one B representation in the SL. Center-zone phonons E and edge-zone modes M_{12} and M_{34} of the oxide fall into the E representation of the SL, and edge-zone phonons M_5 of the oxide, after splitting, contribute to A and B representations of the SL. Components of center-zone phonons T_{2g} and T_{1u} of silicon, after splitting, fall into B and E representations of the SL, and components of the edge-zone phonon X_1, after splitting, fall into A and B representations of the SL, while edge-zone phonons X_3 and X_4, without splitting, fall into E representation of the CP.

Taking into account the scheme of IRR correlation, we can discuss in more details the correspondence between phonons of the SL and component crystals. Table 3 shows corresponding IRRs for all phonons. Our calculation confirms correspondence of phonons that have fallen into the first group in Table 3. Indeed, in this group, four nondegenerated and two doubly-degenerated modes of component crystals are correspondent with the same number of SL modes in strict compliance with Table 2. The second group of SL phonons in Table 3 includes two nondegenerated modes (811 and 720 cm^{-1}), that have corresponding M_{12}-mode (798 cm^{-1}) and E-mode (792 cm^{-1}) in SiO_2. And 3 nondegenerated modes of the SL can be matched with 3 modes in SiO_2: $M_5 + B_1 \rightarrow 2B$, $M_5 \rightarrow A$.

Table 3. Correlation of IRRs in groups of symmetry of SL and component structures

System	Si	$Si_4/(SiO_2)_4$	SiO_2
Sp. group	$Fd\bar{3}m$	$P\bar{4}$	$I\bar{4}2d$
IRR	X_1 →	$9A$	← A_1+2A_2; ← $4M_5$
	X_1 →; T_{2g}, T_{1u} →	$11B$	← $2B_1+3B_2$; ← $4M_5$
	T_{2g}, T_{1u} →; X_3+X_4 →	$14E$	← $5E+2M_{12}+3M_{34}$

In the third and fourth groups 9 degenerated modes of the SL correspond to 8 degenerated modes, and 12 nondegenerated modes correspond to 11 nondegenerated modes of parent crystals. Thus, additional modes with nonzero frequencies appear in the SL spectrum. They are associated with antiphase translation oscillations of atoms in neighboring layers. The search for these modes among the calculated phonon states of the SL made it possible to distinguish two modes with waveforms meeting the condition of antiphase oscillations of interface atoms to the most possible degree. They are shown in Fig. 3.

Since the crystalline silicon has no modes active in IR-spectrum, it is reasonable to suppose that the IR-spectrum of the SL is mainly contributed by the modes localized in the oxide layers. Fig. 4 shows IR-spectra of pure oxide ($\tilde{\beta}$-christobalite) and SL.

According to distribution (3), there are 6 phonon modes ($2B_2 + 4E$) active in the IR-spectrum of $\tilde{\beta}$-christobalite. Three groups of lines can be distinguished in the calculated spectrum (see Fig. 5, b). High-frequency lines ($\sim$ 1100 cm^{-1}) are related to ν_{as} vibrations of O atoms along Si–O–Si bridges. Low-frequency peaks (in the region of 400–450 cm^{-1}) are related to ν_s vibrations of O atoms across Si–O–Si bridges. In cubic β-christobalite, corresponding vibrations form two triply-degenerated modes T_{1u} with frequencies of 1143 and 420 cm^{-1}, respectively [41]. In tetragonal $\tilde{\beta}$-christobalite, each triplet splits into a doublet of nondegenerated B_2-mode and doubly-degenerated E-mode. Value of the frequency splitting in these doublets is the measure of cubic structure distortion in the tetragonal

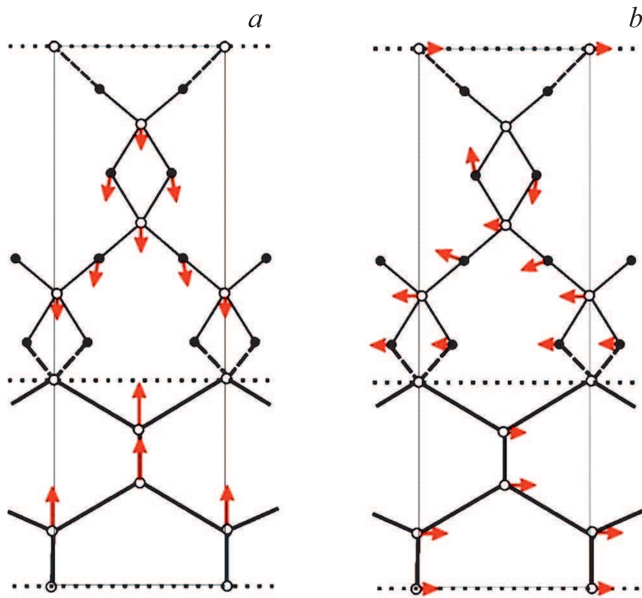

Figure 3. Waveforms of oscillations in the modes that include antiphase translation of neighboring layers are: A-mode 202 cm^{-1} (a) and E-mode 96 cm^{-1} (b). Interface planes are shown by dashed lines.

phase. Another two E-modes with frequencies of 89 and 792 cm^{-1} in the spectrum of $\tilde{\beta}$-christobalite originate from modes T_{2u} and T_{1g} of cubic β-christobalite and become IR-active due to the tetragonal distortion. The intensity of the first of them is almost equal to zero, while the second mode gives a noticeable peak near 800 cm^{-1}, which intensity can be used to assess the degree of tetragonal distortion.

As a matter of form, there are 23 modes $(10B + 13E)$ active in the IR-spectrum of the SL, ten of which originating from center-zone modes, and other 13 originating from edge-zone modes of the $\tilde{\beta}$-christobalite crystal. Actually, there are 10 lines distinguishable in the calculated spectrum (Fig. 4, a) that can be divided into the same three groups of lines. It is worth noting, that in each group we find a considerably larger number of lines, than in the spectrum of $\tilde{\beta}$-christobalite. On the one hand, it is a consequence of cell broadening, and on the other hand it is caused by the change in rules of selection related to the decrease in symmetry. Also, it is worth noting, the considerably increased splitting, which is a consequence of elastic deformations arising in the oxide when the heterostructure is formed.

The manifestation of lines 720 and 811 in the IR-spectrum of the SL can be used for the spectroscopic identification of this type of interface. According to Table 3, these lines are related to E-modes, one of which originates from the center-zone E-mode (792 cm^{-1}), and the send mode originates from the edge-zone phonon M_{12} (798 cm^{-1}) $\tilde{\beta}$-christobalite. These modes are mixed in the SL spectrum, which causes such a strong frequency splitting. Mixed character of these modes suggests that their positions in the spectrum will change significantly with changes in the thickness of the oxide layer.

The interpretation of RS-spectrum is more complex because RS-active modes exist in both materials. The Si crystal has one such mode in the T_{1g} IRR. It is triply-degenerated and in the unstressed crystal in the calculation it has a frequency of 502 cm^{-1}. In the $\tilde{\beta}$-christobalite there are 13 RS-active modes (all modes are active except for the two modes with A_2 symmetry). As a result, we can expect in the SL spectrum the presence of 16 lines originating from center-zone modes of component crystals. In addition, due to the summation of phonon branches and disturbance of selection rules in the RS-spectrum of the SL, also the modes can become active, that are related to edge-zone phonons of component crystals. In principle, all 45 modes are resolved in the RS-spectrum in the $Si_4/(SiO_2)_4$ SL.

According to estimate (1), elastic deformations of the silicon layer should decrease the upper boundary of the frequency range by approximately 50 cm^{-1}, i.e., down to $\sim$ 450 cm^{-1}. In the Raman spectrum of the SL (see Fig. 5, a), the group of lines near 350 to 450 cm^{-1} prevails. In this range 3 branches of silicon and 3 branches of oxide are overlapped. The most intensive are two A-modes that give the peaks of 349 and 393. It is reasonable to assume that modes have mixed character in this range. The analysis of oscillation waveforms has confirmed this and demonstrated that the biggest contribution to the first mode gives the X_1 phonon of the silicon layer, and the second mode is mainly contributed by the type ν_2 deformation oscillation of the oxide layer. The Raman peak of 454 at the first boundary of this group of lines contains contributions of the A-mode (458 cm^{-1}) and the E-mode (453 cm^{-1}), that arise as a result of splitting of the T_{1g}-mode in the material of the silicon layer.

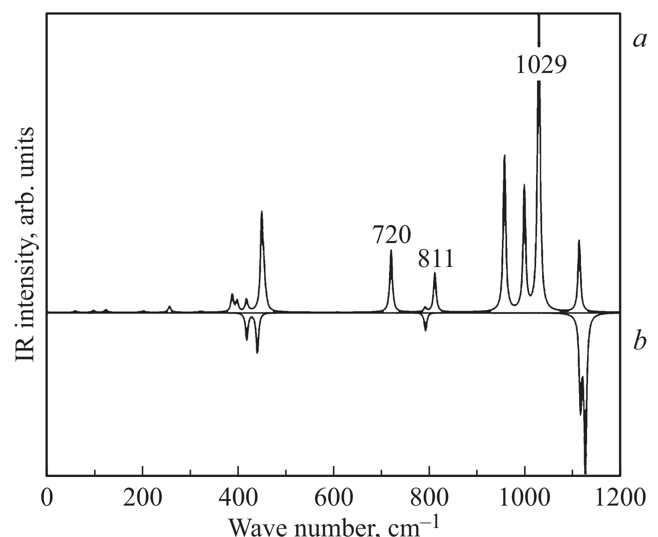

Figure 4. Calculated IR-spectra of the SL $Si_4/(SiO_2)_4$ (a) and $\tilde{\beta}$-christobalite (b).

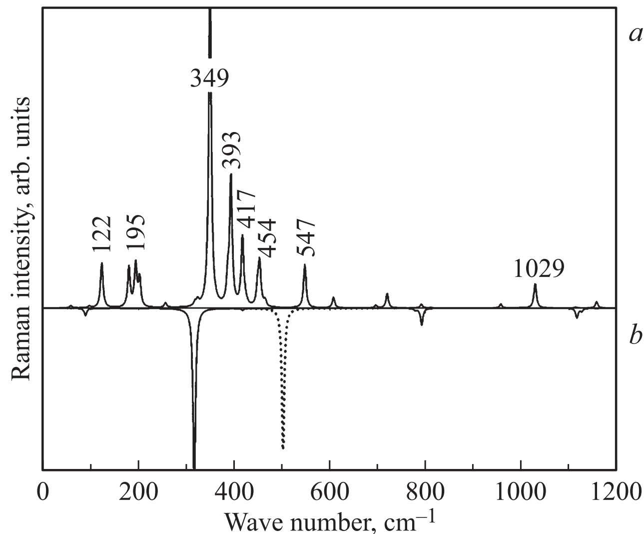

Figure 5. Calculated RS-spectra of the SL of $Si_4/(SiO_2)_4$ (a), $\tilde{\beta}$-christobalite (solid line) and silicon (dashed line) (b).

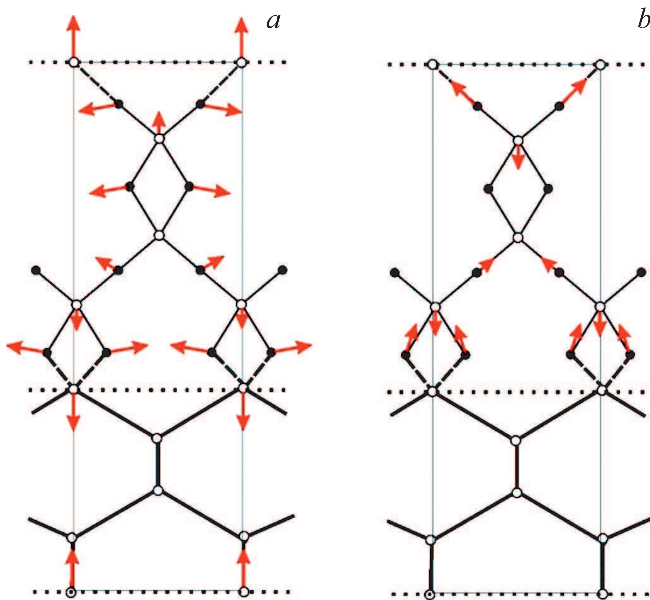

Figure 6. Waveforms of oscillations in the A-mode of $547\,cm^{-1}$ (a) and the B-mode of $1029\,cm^{-1}$ (b). Interface planes are shown by dashed lines.

In the modes with frequencies higher than $460\,cm^{-1}$, the contribution of silicon layer oscillations is negligible. Thus, for example, the peak of 547 is related to the A-mode originating from the deformation oscillation in the oxide layer, while the peak of 1029 is related to the B-phonon including ν_{as}(Si–O) oscillations localized in Si–O–Si bridges near the interface layer.

The most interesting for the spectroscopic characterization of the SL is the A-mode of $547\,cm^{-1}$, giving a noticeable peak in the region without lines from component crystals spectra. This mode (see Fig. 6, a) is related to an edge-zone phonon (M_5-mode) of the oxide and is an antiphase expansion/compression of neighboring layers along the SL axis. Frequency of this mode should be strongly dependent on the thickness of layers, which can be used for the spectroscopic characterization of the SL structure.

Another spectroscopic mark of the presence of this interface type can be the peak of 1029, which is related to ν_{as}(Si–O) oscillations localized in Si–O–Si bridges near the interface layer (see Fig. 6, b). In addition, this mode gives a strong line in the IR-spectrum (see Fig. 4).

We have made an attempt to compare the calculated RS-spectrum of the SL with the only experimental spectrum available from literature [11]. In general, it can be said that they match each other. In the experimental RS-spectrum a wide band from 300 to $550\,cm^{-1}$ is predominant, which has a corresponding set of intensive peaks from 349 to 547 in the calculation. In the experiment less intensive peaks were observed at 620 and $800\,cm^{-1}$, that can be matched with B-modes with frequencies of 608 and $791\,cm^{-1}$ in the calculation. The observed band of $950-1000\,cm^{-1}$ in the experiment can be matched with four modes from the first group (see Table 2). And finally, two high-frequency peaks observed at 1090 and $1200\,cm^{-1}$ correspond to A and B modes with frequencies of 1114 and $1157\,cm^{-1}$ in the calculation. Note that the quantitative difference between frequencies of observed peaks and calculated modes may be explained by the size effect: the experimental spectrum was measured at a sample with a thick (60 nm) oxide layer on a silicon substrate, and the model structure used in the calculation had thicknesses of oxide and silicon layers less than 1 nm. For more robust comparison with this experiment, it is necessary to study the dependence of calculated spectrum on the thickness of layers.

4. Conclusion

We have investigated instabilities arising in the case of juncture of silicon and β-christobalite crystals through (001) surfaces. It is shown that this method of juncture of two materials ensures maximum thin interface of one monolayer of the silicon lattice. It is shown that due to the high lability of the β-christobalite crystalline lattice it can relax into a new structure keeping the stability of the sharp interface. Types of structural instabilities were examined that arise in the silicon/christobalite SL due to mismatching of sizes of the two lattices. All unstable phonon modes are determined and for each of them relaxation of structure is performed until detection of a stable distorted configuration. The stable structures are found. It is shown that the silicon layer in all relaxed structures keeps a slightly deformed ideal crystalline structure, and the oxide layer structure has considerable internal rebuilding in addition to uniform deformations. Structural flexibility of the christobalite lattice is ensured by the presence of a large number of RUMs. We have shown in this study that in all relaxed SLs the

structure of an oxide layer can be considered as a lattice of β-christobalite distorted along one of the RUMs.

Comparison of energies of the found distorted structures made it possible to distinguish the most asymmetric structure with the lowest energy and the second structure with a bit higher energy, but with a symmetry keeping the fourth order axis. It is found that symmetry of such SL corresponds to space group $P\bar{4}$. The rest of this study represents the results of simulation of phonon states and vibration spectra of the $Si_4/(SiO_2)_4$ SL with a symmetry of group $P\bar{4}$. It is shown that in this structure the oxide layer build-up is similar to the polymorphic modification known as $\tilde{\beta}$-christobalite. The analysis of the calculated eigenvectors of the SL has shown that high-frequency modes (higher than $500\,cm^{-1}$) are completely localized in the oxide layer. Atoms of the silicon layer participate in oscillations with lower frequencies and have the biggest amplitudes in modes with frequencies in the range of $350-450\,cm^{-1}$. Interface atoms of Si (bonded with two atoms of O and two atoms of the silicon layer) have the biggest amplitudes in the oscillations with frequencies in the range of $400-700\,cm^{-1}$. The issue of impact of elastic strains on phonons localized in the silicon layer is investigated. The estimate of frequency shift obtained by us using the deformation potentials available in literature corresponds to the frequency lowering by $\sim 50\,cm^{-1}$, which is confirmed by the results of our ab initio calculations. The calculated IR- and RS-spectra of the SL were analyzed to identify spectral features that can be used for the spectroscopic identification of such structures. A line near $720\,cm^{-1}$ is found in the IR-spectrum of the SL, that originates from the nonpolar B_1-mode of the bulk oxide and becomes IR-active in the structure of the SL. This line is convenient for observation because there are no other IR-lines near it in the oxide spectrum nor in the silicon spectrum. Its intensity and frequency can be used to estimate the degree of tetragonal distortion. Two lines are distinguished in the IR-spectrum that are the most interesting for the spectroscopic characterization of the SL. The A-mode with a frequency of $547\,cm^{-1}$ gives a noticeable peak in the range where there are no lines from component crystals spectra. This mode is an antiphase expansion/compression of neighboring layers along the SL axis. Its frequency and intensity should be strongly dependent on the thicknesses of SL layers. Another spectroscopic mark of presence of this interface type can be the RS-peak at a frequency of $1029\,cm^{-1}$, related to the B-mode composed of valence vibration localized in Si$-$O$-$Si bridges in the close vicinity of the interface layer. The comparison of our calculation results with the available experimental data for RS-spectra [10] allows for the conclusion that they match well to each other.

The main result of this study is that using ab initio calculation methods of computer simulation a stable structure of Si/SiO_2 SL with sharp interface is found for the first time. Its phonon states, IR- and RS-spectra are examined, where characteristic lines are found that can be used to detect the presence of this interface type in the samples in question.

Funding

The study was supported by a grant of the Russian Science Foundation (project No. 22-22-20021) using resources of the Computer Center of the Saint-Petersburg State University and the Computer Center of the I.F. Ioffe Physical-Technical Institute.

Conflict of interest

The authors declare that they have no conflict of interest.

References

[1] S.T. Pantelides. Mater. Sci. Forum **527-529**, 935 (2006).
[2] Z.H. Lu, D.J. Lockwood, J.-M. Baribeau. Nature **378**, 258 (1995).
[3] N. Liu, J. Sun, S. Pan, Z. Chen, W. Shi, R. Wang, X. Wang. Opt. Commun. **176**, 239 (2000).
[4] T. Zheng, Z. Li. Superlat. Microstruct. **37**, 227 (2005).
[5] S. Yamada, M. Konagai, S. Miyajima. Jpn. J. Appl. Phys. **55**, 04ES06 (2016).
[6] L. Khriachtchev, M. Räsänen, S. Novikov, O. Kilpelä, J. Sinkkonen. J. Appl. Phys. **86**, 5601 (1999).
[7] M. Benyoucef, M. Kuball, J.M. Sun, G.Z. Zhong, X.W. Fan. J. Appl. Phys. **89**, 7903 (2001).
[8] B. Jin, X. Wang, J. Chen, X. Cheng, Z. Chen. Appl. Phys. Lett. **87**, 051921 (2005).
[9] S. Novikov, J. Sinkkonen, L. Khriachtchev, M. Räsänen, A. Sitnikova. Proc. SPIE **6195**, 619512 (2006).
[10] S. Huang, H. Xiao, S. Shou. Appl. Surf. Sci. **255**, 4547 (2009).
[11] P. Borowicz, M. Latek, W. Rzodkiewicz, A. Łaszcz, A. Czerwinski, J. Ratajczak. Adv. Nature Sci.: Nanosci. Nanotechnol. **3**, 045003 (2012).
[12] S. Yamada, M. Konagai, S. Miyajima. Jpn. J. Appl. Phys. **55**, 04ES06 (2016).
[13] F. Herman, R.V. Kasowski. J. Vac. Sci. Technol. **19**, 395 (1981).
[14] M. Hane, Y. Miyamoto, A. Oshiyama. Phys. Rev. B **41**, 12637 (1990).
[15] A. Pasquarello, M.S. Hybertsen, R. Car. Appl. Phys. Lett. **68**, 625 (1996).
[16] N. Tit, M.W.C. Dharma-wardana. Solid State Commun. **106**, *3*, 121 (1998).
[17] R. Buczko, S.J. Pennycook, S.T. Pantelides. Phys. Rev. Lett. **84**, 943 (2000).
[18] E. Degoli, S. Ossicini. Surf. Sci. **470**, 32 (2000).
[19] T. Yamasaki, C. Kaneta, T. Uchiyama, T. Uda, K. Terakura. Phys. Rev. B **63**, 115314 (2001).
[20] P. Carrier, L.J. Lewis, M.W.C. Dharma-wardana. Phys. Rev. B **65**, 165339 (2002).
[21] M. Watarai, J. Nakamura, A. Natori. Phys. Rev. B **69**, 035312 (2004).
[22] F. Giustino, A. Bongiorno, A. Pasquarello. J. Phys.: Condens. Matter **17**, S2065 (2005).
[23] Y. Yamashita, S. Yamamoto, K. Mukai, J. Yoshinobu1 Y. Harada, T. Tokushima, T. Takeuchi, Y. Takata, S. Shin, K. Akagi, S. Tsuneyuki. Phys. Rev. B **73**, 045336 (2006).
[24] K. Seino, J.-M. Wagner, F. Bechstedt. Appl. Phys. Lett. **90**, 253109 (2007).
[25] S. Markov, P.V. Sushko, S. Roy, C. Fiegna, E. Sangiorgi, A.L. Shluger, A. Asenov. Phys. Status Solidi A **205**, 1290 (2008).

[26] M. Ribeiro, L.R.C. Fonseca. Phys. Rev. B **79**, 241312R (2009).
[27] K. Seino, F. Bechstedt. Semicond. Sci. Technol. **26**, 014024 (2011)
[28] S. Markov, C. Yam, G. Chen, B. Aradi, G. Penazzi, T. Frauenheim. In: Int. Conf. on Simulation of Semiconductor Processes and Devices (2014), P. 65–68.
[29] F. Zheng, H.H. Pham, L-W. Wang. Phys. Chem. Chem. Phys. **19**, 32617 (2017).
[30] P. Li, Y. Song, X. Zuo. Phys. Status Solidi RRL **13**, *3*, 1800547 (2018)
[31] M. Jech, A-M. El-Sayed, S. Tyaginov, A.L. Shluger, T. Grasser. Phys. Rev. B **100**, 195302 (2019)
[32] J.P. Perdew, A. Ruzsinszky, G.I. Csonka, O.A. Vydrov, G.E. Scuseria, L.A. Constantin, X. Zhou, K. Burke. Phys. Rev. Lett. **100**, 136406 (2008).
[33] X. Gonze, J.M. Beuken, R. Caracas, F. Detraux, M. Fuchs, G.M. Rignanese, L. Sindic, M. Verstraete, G. Zerah, F. Jollet, M. Torrent, A. Roy, M. Mikami, Ph. Ghosez, J.-Y. Raty, D.C. Allan. Comput. Mater. Sci. **25**, 478 (2002).
[34] X. Gonze, G.M. Rignanese, M. Verstraete, J.M. Beuken, Y. Pouillon, R. Caracas, F. Jollet, M. Torrent, G. Zerah, M. Mikami, P. Ghosez, M. Veithen, J.-Y. Raty, V. Olevano, F. Bruneval, L. Reining, R. Godby, G. Onida, D.R. Hamann, D.C. Allan. Z. Krist. **220**, 558 (2005).
[35] X. Gonze, B. Amadon, P-M. Anglade, J-M. Beuken, F. Bottin, P. Boulanger, F. Bruneval, D. Caliste, R. Caracas, M. Côté, T. Deutsch, L. Genovese, Ph. Ghosez, M. Giantomassi, S. Goedecker, D.R. Hamann, P. Hermet, F. Jollet, G. Jomard, S. Leroux, M. Mancini, S. Mazevet, M.J.T. Oliveira, G. Onida, Y. Pouillon, T. Rangel, G.-M. Rignanese, D. Sangalli, R. Shaltaf, M. Torrent, M.J. Verstraete, G. Zerah, J.W. Zwanziger. Comput. Phys. Commun. **180**, 2582 (2009).
[36] D.R. Hamann. Phys. Rev. B **88**, 085117 (2013).
[37] H.J. Monkhorst, J.D. Pack. Phys. Rev. B **13**, 5188 (1976).
[38] X. Gonze, C. Lee. Phys. Rev. B **55**, 10355 (1997).
[39] X. Gonze, J.P. Vigneron. Phys. Rev. B **39**, 13120 (1989).
[40] M. Smirnov, P. Saint-Gregoire. In: Perovskites and other Framework Structure Crystalline Materials. Collaborating Academics (2021) P. 355–372.
[41] S. Coh, D. Vanderbilt. Phys. Rev. B **78**, 054117 (2008).
[42] E. Jette, F. Foote. J. Chem. Phys. **3**, 605 (1935).
[43] T. Demuth, Y. Jeanvoine, J. Hafner, J.G. Angyan. J. Phys.: Cond. Matter. **11**, 3833(1999).
[44] A.F. Wright, A.J. Leadbetter. Phil. Mag. **31**, 1391 (1975).
[45] P. Giannozzi, S. Gironcoli, P. Pavone, S. Baroni. Phys. Rev. B **43**, 7231(1991).
[46] G. Nilsson, G. Nelin. Phys. Rev. B **6**, 3777 (1972).
[47] J.B. Bates. J. Chem. Phys. **57**, 4042 (1972).
[48] S. Nakashima, T. Mitani, M. Ninomiya, K. Matsumoto. J. Appl. Phys. **99**, 053512 (2006).
[49] C.-Y. Peng, C.-F. Huang, Y.-C. Fu, Y.-H. Yang, C.-Y. Lai, S.-T. Chang, C.W. Liu. Appl. Phys. Lett. **104**, 031106 (2014).
[50] D.C. Palmer, R.J. Hemley, Ch.T. Prewitt. Phys. Chem. Minerals **21**, 481 (1994).